

Supplementary Information

Tuning Electron Affinity of Cobalt Oxide Catalysts for Robust Acidic Oxygen Evolution

Ruo-Zi Fang^a, Xin-Yi Wan^a, Jun-Sheng Chen^a, Youmin Hou^b, Bin Hua^{a,}*

^a Key Lab of Artificial Micro- and Nano-Structures of Ministry of Education, School of Physics and Technology, Wuhan University, Wuhan, Hubei 430072, China

* Corresponding author: bin.hua@whu.edu.cn

^b School of Power and Mechanical Engineering, Wuhan University, Wuhan, Hubei 430072, China.

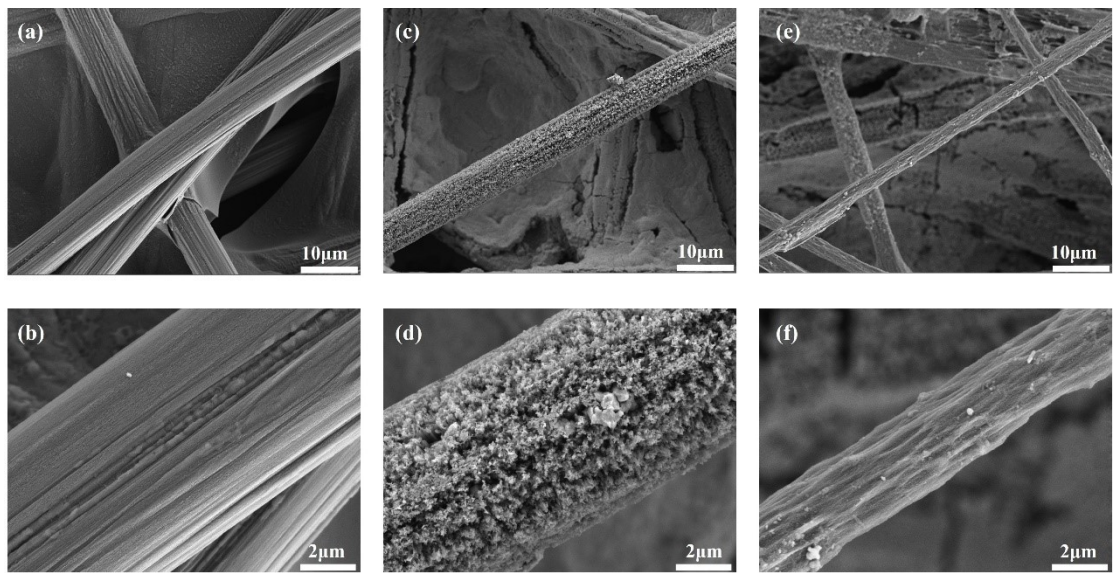


Figure S1. SEM images of (a,b) Carbon paper, (c,d) before and (e,f) after testing 180h of Mo-Co₃O₄ catalyst.

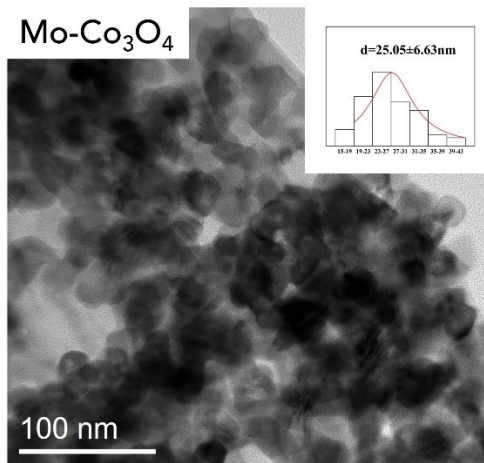


Figure S2. TEM image of Mo-Co₃O₄ catalyst and the corresponding particle size distribution map.

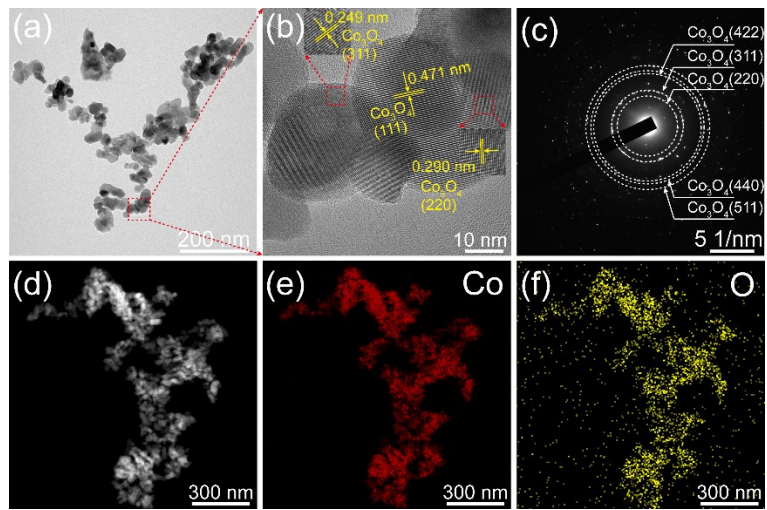


Figure S3. (a) TEM images, (b) HRTEM images, (c) SAED pattern, (d-f) HAADF-STEM and corresponding elemental mappings of Co_3O_4 .

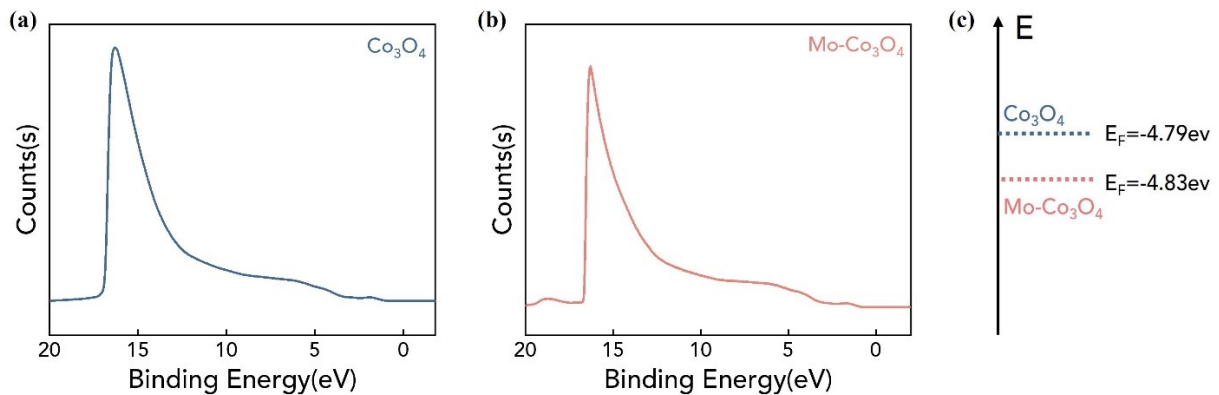


Figure S4. UPS of (a) Co_3O_4 , (b) $\text{Mo}-\text{Co}_3\text{O}_4$ and (c) Schematic of the calculated Fermi level.

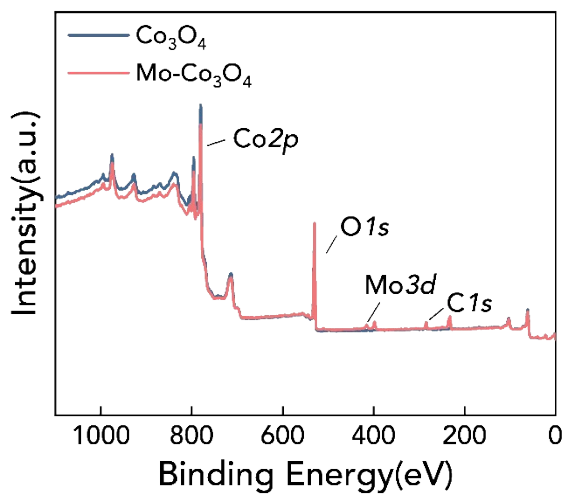


Figure S5. XPS survey spectra of prepared samples.

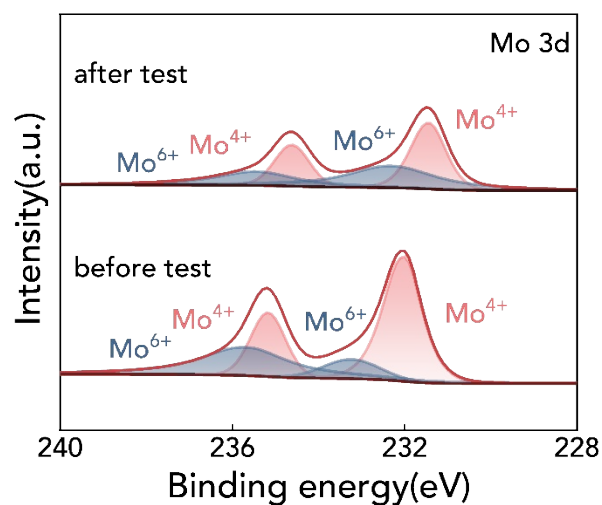


Figure S6. XPS Mo 3d spectra of before and after testing 20h of Mo-Co₃O₄ catalyst.

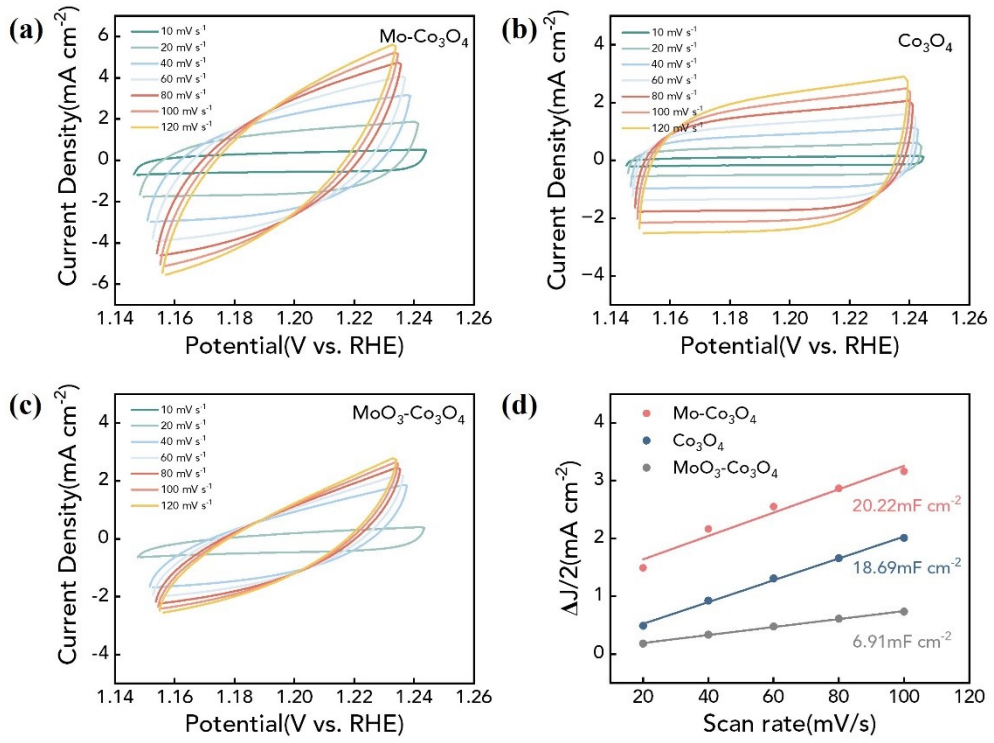


Figure S7. Cyclic voltammograms of (a) Mo-Co₃O₄, (b) Co₃O₄, (c) MoO₃-Co₃O₄ at different scan rates, and (d) Double layer capacitance (C_{dl}).

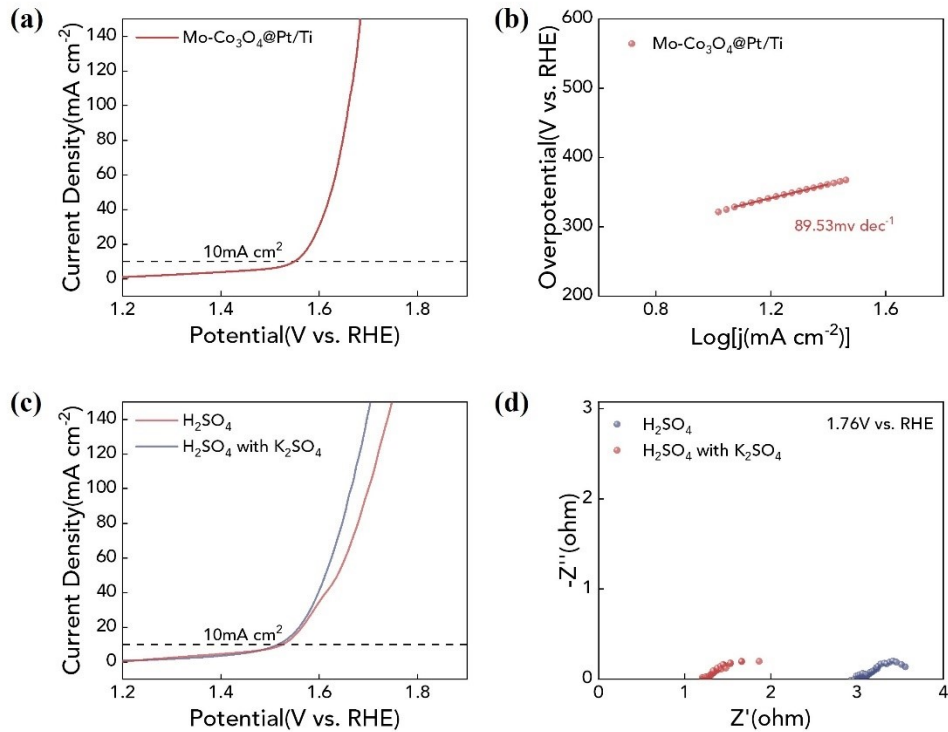


Figure S8. (a) LSV curves and (b) Tafel slope plots of. (c) LSV curves and (d) EIS profiles of $\text{Mo-Co}_3\text{O}_4$ in H_2SO_4 (pH 0.3) and H_2SO_4 with $0.5 \text{ M K}_2\text{SO}_4$ (pH 0.3).

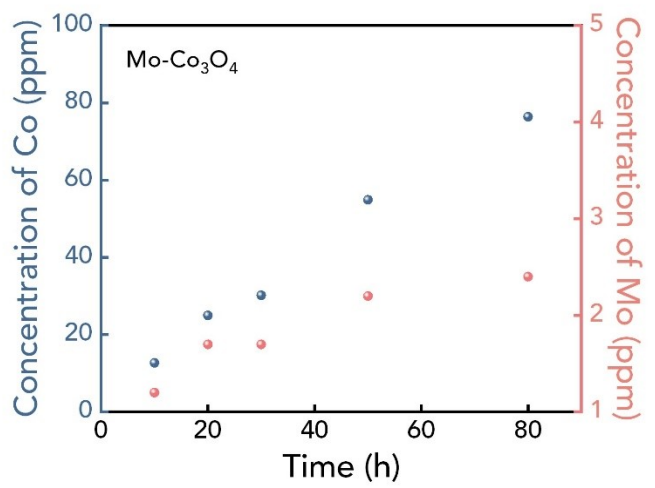


Figure S9. Elemental leaching assessed by ICP-OES of Mo-Co₃O₄ for the electrolyte after a continuous test at 10 mA·cm⁻² for 80 h.

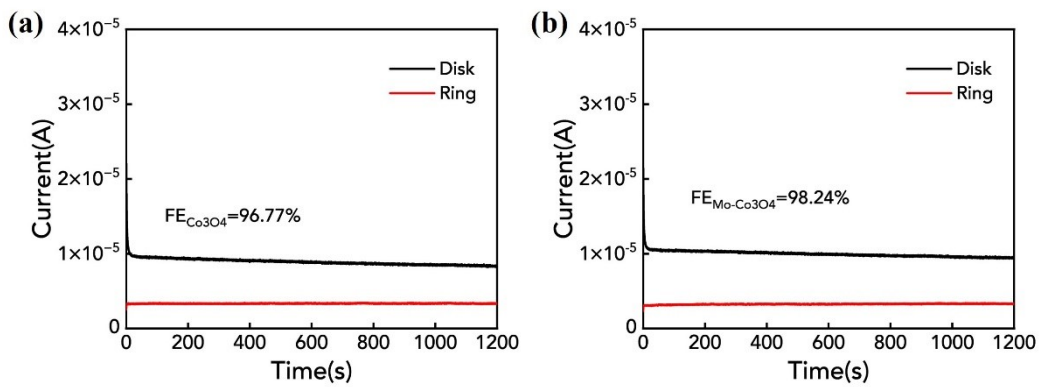


Figure S10. The Faraday efficiency (FE) of (a) Co_3O_4 and (b) $\text{Mo}-\text{Co}_3\text{O}_4$ was calculated by collecting the current of the disk electrode and the ring electrode.

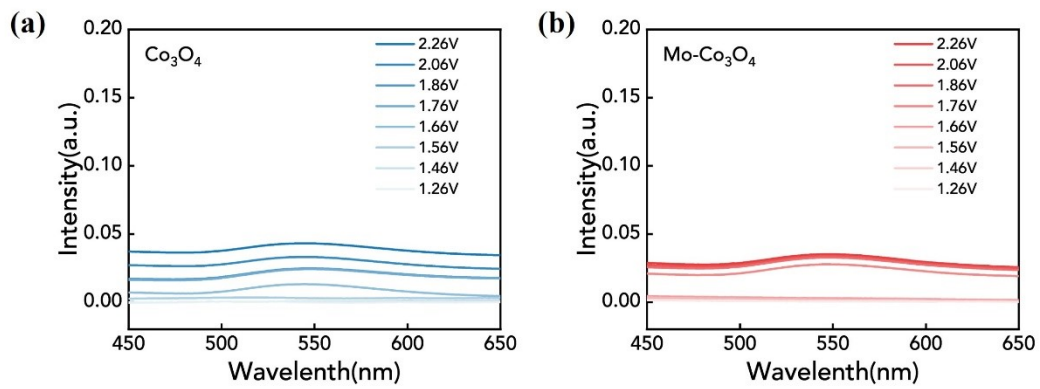


Figure S11. UV-Vis absorption spectra of the electrolyte of (a) Co₃O₄ (b) Mo-Co₃O₄ at 1.26-2.26 V vs. RHE.

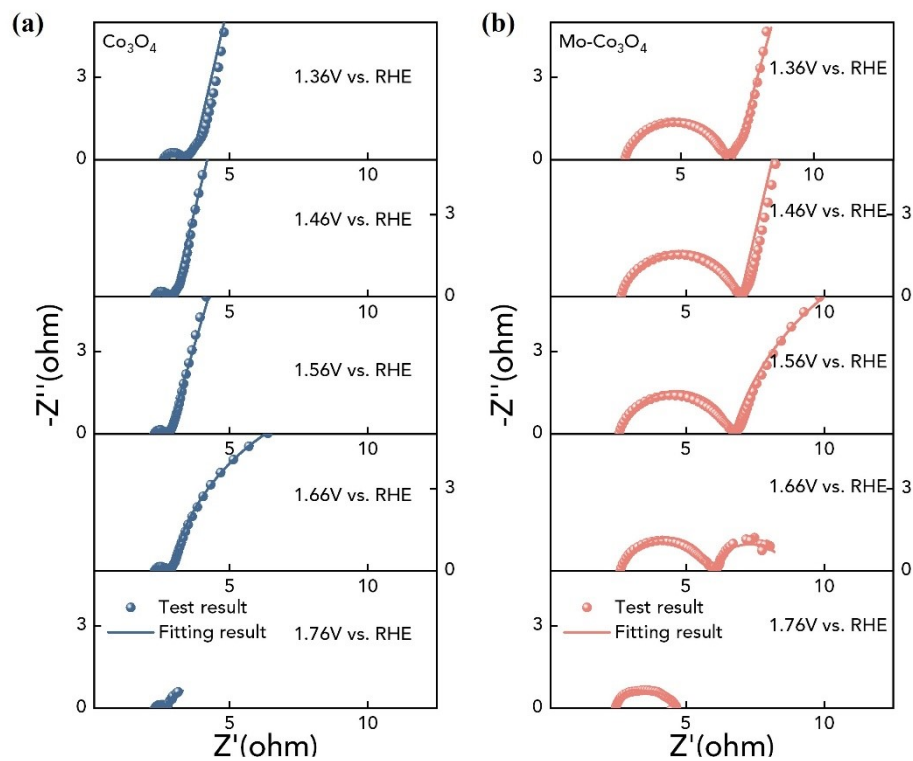


Figure S12. EIS Nyquist fitting curves of (a) Co_3O_4 and (b) $\text{Mo}-\text{Co}_3\text{O}_4$ recorded from 1.36 V to 1.76 V vs. RHE

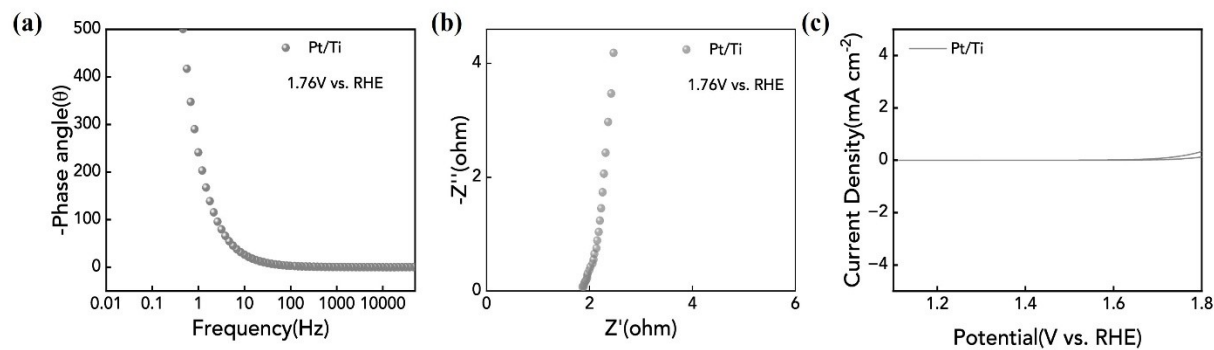


Figure S13. (a) Bode plots (b) Nyquist plots and (c) CV for Pt/Ti

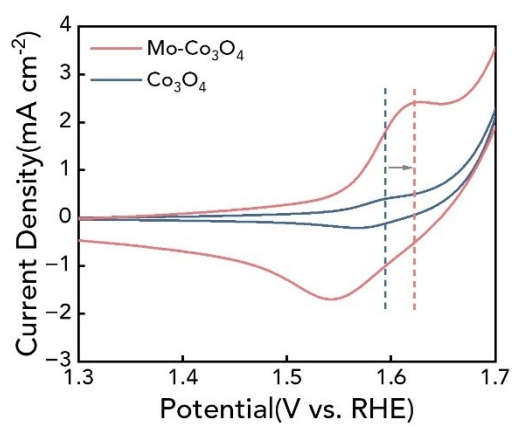


Figure S14. CV curves of Mo-Co₃O₄ and Co₃O₄ tested on a rotating ring-disk electrode.

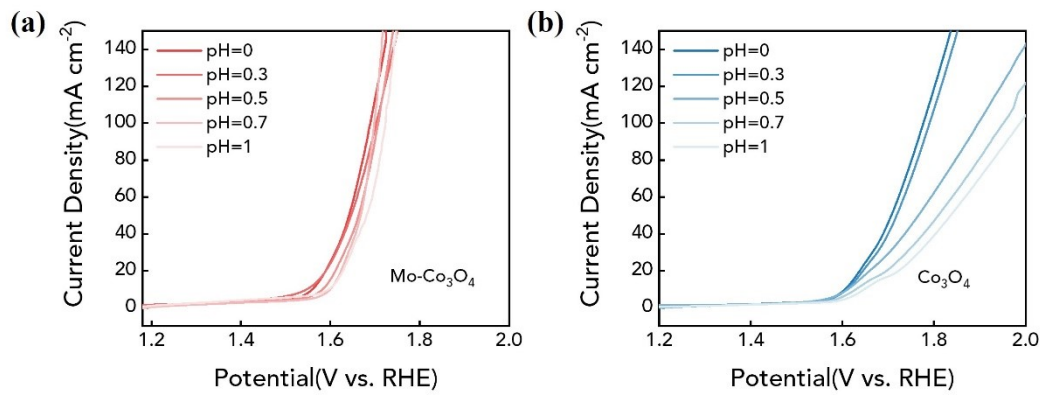


Figure S15. (a) Mo-Co₃O₄ and (b) Co₃O₄ in acid electrolytes with different pH values.

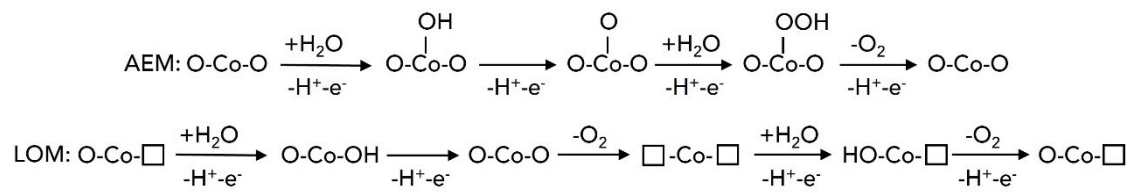


Figure S16. Diagram of AEM and LOM paths.

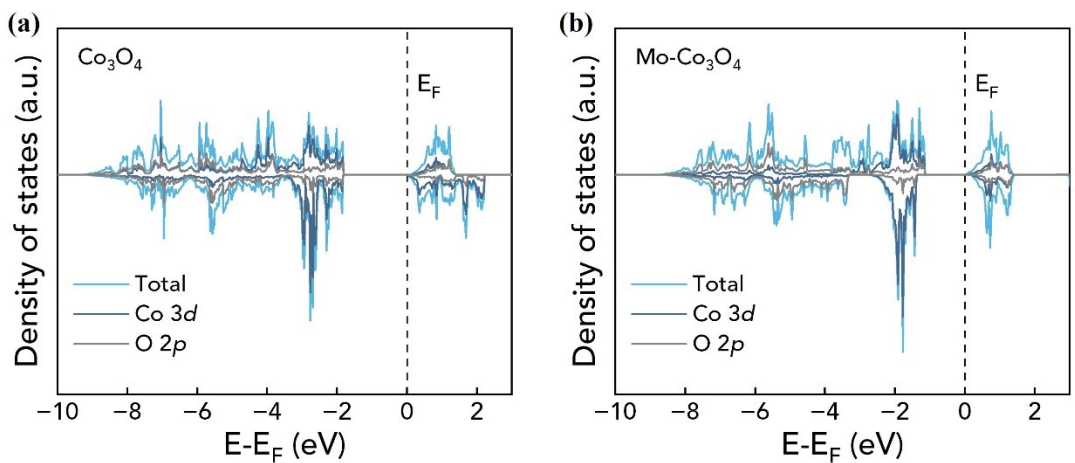


Figure S17. The curves of density of states of Co 3d and O 2p orbitals in (a) Co_3O_4 and (b) $\text{Mo}-\text{Co}_3\text{O}_4$.

Table S1. The fitting results of XRD tests on (220) planes

	2θ	w	Interfacial	Lattice	Mean particle	Cell
			spacing (nm)	parameter (nm)	size (nm)	
Mo-Co ₃ O ₄	31.3140	0.3517	0.28543	0.80730	23.1980	
Co ₃ O ₄	31.3124	0.3433	0.28544	0.80734	23.7649	Cubic

Table S2. Different peak positions and contents of Co 2p XPS spectra for samples

Sample	Co ²⁺	Co ³⁺
	2p _{3/2} /2p _{1/2} (eV)	2p _{3/2} /2p _{1/2} (eV)
Co ₃ O ₄	781.3eV/796.5eV	780eV/795eV
Mo-Co ₃ O ₄	781.5eV/796.7eV	780.2eV/795.2eV
Mo-Co ₃ O ₄ after testing 50h	780.8eV/796.3eV	779.6eV/794.7eV

Table S3. Different peak positions of Mo 3d XPS spectra for samples

Sample	Mo⁴⁺	Mo⁶⁺
	3d_{3/2}/3d_{1/2}(eV)	3d_{3/2}/3d_{1/2}(eV)
Mo-Co ₃ O ₄	232eV/235.1eV	233.2eV/235.7eV
Mo-Co ₃ O ₄ after testing 50h	231.5eV/234.6eV	232.4eV/235.5eV

Table S4. Different peak positions and contents of O 1s XPS spectra for samples

Sample	O _{M-O} (eV/100%)	O _V (eV/100%)	O _{M-OH} (eV/100%)	O _V / O _{M-O}
Co ₃ O ₄	529.6eV/81.9	531.2eV/13.3	532.2eV/4.8	0.16
Mo-Co ₃ O ₄	530.1eV/64.7	531.6eV/28.5	532.7eV/6.8	0.44
Mo-Co ₃ O ₄ after testing 50h	530.1eV/64.1	531.3eV/27.5	532.8eV/8.4	0.43

Table S5. OER performance of as-synthesized electrodes in this work

Catalysts	η_{10} (mV)	Tafel slope (mV dec ⁻¹)	R_{ct} (Ω)	Cdl (mF cm ⁻²)	Durable time @10mA cm ⁻² (h)
Co ₃ O ₄	432	107.01	1.70	18.69	50
MoO ₃ -Co ₃ O ₄	496	127.02	2.23	6.91	40
Mo-Co ₃ O ₄	348	84.32	1.32	20.22	More than 180

Table S6. A summary of Stability of Mo-Co₃O₄ and other reported Co based catalysts in acidic electrolyte

Catalysts	Electrolyte	Stability @ Current		References
		density (h@ mA cm ⁻²)		
Mo-Co ₃ O ₄	0.5M H ₂ SO ₄	180/10		This work
Mo-Co ₃ O ₄	0.5M H ₂ SO ₄	300/50		This work
Amorphous CoFeO _x	pH 2 in Pi	2/1		2 ^[2]
Amorphous CoPbO _x	pH 2.5 in Pi	8/1		2 ^[2]
Amorphous CoFePbO _x	pH 2 in Pi	50/1		2 ^[2]
Co ₂ TiO ₄	0.5M H ₂ SO ₄	10/5		3 ^[3]
Crystalline Co ₃ O ₄	0.5M H ₂ SO ₄	15/10		4 ^[4]
Mn-doped FeP/Co ₃ (PO ₄) ₂	0.5M H ₂ SO ₄	8.3/5		5 ^[5]
Co ₃ O ₄ @C	1M H ₂ SO ₄	40/10		6 ^[6]
Co ₃ O ₄ /CeO ₂	0.05M H ₂ SO ₄	100/10		7 ^[7]
CoFePbO _x	1M H ₂ SO ₄	13/100		8 ^[8]
CoFe	1M H ₂ SO ₄	2/10		9 ^[9]
Co _{0.05} Fe _{0.95} O _y	pH 0.3 H ₂ SO ₄	50/10		10 ^[10]
CoFePbO _x	pH 0 H ₂ SO ₄	14/10		8 ^[8]
Ag-doped Co ₃ O ₄	0.5M H ₂ SO ₄	10/6.5		11 ^[11]
Co ₃ (PO ₄) ₂	1M H ₃ PO ₄	30/1.8		12 ^[12]
Ir-Co ₃ O ₄	0.5M H ₂ SO ₄	6/50		13 ^[13]
La and Mn doped Co ₃ O ₄	0.1M HClO ₄	300/10		14 ^[14]
Co ₂ MnO ₄	pH 1 H ₂ SO ₄	200/100		15 ^[15]
Co _{3-x} Ba _x O ₄	0.5M H ₂ SO ₄	100/10		16 ^[16]

Table S7. The detailed data of ICP-OES after the stability test of Mo-Co₃O₄

Test time (h)	Concentration of dissolved elements in electrolyte (ppm)		Degradation rate (mV h ⁻¹)	Dissolution rate of Co (ppm h ⁻¹)
	Co	Mo		
10	12.7	1.2		
20	25	1.7		
30	30.2	1.7	0.47	1.098
50	54.9	2.2		

Table S8. The detailed data of ICP-OES after the stability test of Co₃O₄

Test time (h)	Concentration of dissolved Co in electrolyte (ppm)	Degradation rate (mV h ⁻¹)	Dissolution rate of Co (ppm h ⁻¹)
10	13.6		
20	27.2		
30	41.2	2.175	1.336
50	66.8		

Table S9. Optimum fit parameters for the impedance date of Co₃O₄ during OER in 0.5M H₂SO₄

E (V vs. RHE)	R _s (Ω)	R1 (Ω)	R2 (Ω)
1.36	2.587	1.105	1.925×10 ⁹
1.46	2.283	0.674	3.438×10 ⁷
1.56	2.313	0.483	135.3
1.66	2.315	0.533	16.17
1.76	2.328	0.352	2.099

Table S10. Optimum fit parameters for the impedance date of Mo-Co₃O₄ during OER in 0.5M H₂SO₄

E (V vs. RHE)	R _s (Ω)	R1 (Ω)	R2 (Ω)
1.36	2.931	3.933	1.797×10^{10}
1.46	2.704	4.262	3.739×10^8
1.56	2.639	4.046	19.122
1.66	2.673	3.257	2.815
1.76	2.508	0.601	1.530

Reference

- (1) Li, R.-Q.; Wang, B.-L.; Gao, T.; Zhang, R.; Xu, C.; Jiang, X.; Zeng, J.; Bando, Y.; Hu, P.; Li, Y.; Wang, X.-B. Monolithic Electrode Integrated of Ultrathin NiFeP on 3D Strutted Graphene for Bifunctionally Efficient Overall Water Splitting. *Nano Energy* **2019**, *58*, 870–876.
- (2) Huynh, M.; Ozel, T.; Liu, C.; Lau, E. C.; Nocera, D. G. Design of Template-Stabilized Active and Earth-Abundant Oxygen Evolution Catalysts in Acid. *Chem. Sci.* **2017**, *8* (7), 4779–4794.
- (3) Anantharaj, S.; Karthick, K.; Kundu, S. Spinel Cobalt Titanium Binary Oxide as an All-Non-Precious Water Oxidation Electrocatalyst in Acid. *Inorg. Chem.* **2019**, *58* (13), 8570–8576.
- (4) Mondschein, J. S.; Callejas, J. F.; Read, C. G.; Chen, J. Y. C.; Holder, C. F.; Badding, C. K.; Schaak, R. E. Crystalline Cobalt Oxide Films for Sustained Electrocatalytic Oxygen Evolution under Strongly Acidic Conditions. *Chem. Mater.* **2017**, *29* (3), 950–957.
- (5) Liu, H.; Peng, X.; Liu, X.; Qi, G.; Luo, J. Porous Mn-doped FeP/Co₃(PO₄)₂ Nanosheets as Efficient Electrocatalysts for Overall Water Splitting in a Wide pH Range. *ChemSusChem* **2019**, *12* (7), 1334–1341.
- (6) Yu, J.; Garcés-Pineda, F. A.; González-Cobos, J.; Peña-Díaz, M.; Rogero, C.; Giménez, S.; Spadaro, M. C.; Arbiol, J.; Barja, S.; Galán-Mascarós, J. R. Sustainable Oxygen Evolution Electrocatalysis in Aqueous 1 M H₂SO₄ with Earth Abundant Nanostructured Co₃O₄. *Nat Commun* **2022**, *13* (1), 4341.
- (7) Huang, J.; Sheng, H.; Ross, R. D.; Han, J.; Wang, X.; Song, B.; Jin, S. Modifying Redox Properties and Local Bonding of Co₃O₄ by CeO₂ Enhances Oxygen Evolution Catalysis in Acid. *Nat Commun* **2021**, *12* (1), 3036.
- (8) Chatti, M.; Gardiner, J. L.; Fournier, M.; Johannessen, B.; Williams, T.; Gengenbach, T. R.; Pai, N.; Nguyen, C.; MacFarlane, D. R.; Hocking, R. K.; Simonov, A. N. Intrinsically Stable In Situ Generated Electrocatalyst for Long-Term Oxidation of Acidic Water at up to 80 °C. *Nat. Catal.* **2019**, *2* (5), 457–465.
- (9) McCrory, C. C. L.; Jung, S.; Ferrer, I. M.; Chatman, S. M.; Peters, J. C.; Jaramillo, T. F. Benchmarking Hydrogen Evolving Reaction and Oxygen Evolving Reaction Electrocatalysts for Solar Water Splitting Devices. *J. Am. Chem. Soc.* **2015**, *137* (13), 4347–4357.
- (10) Kwong, W. L.; Lee, C. C.; Shchukarev, A.; Messinger, J. Cobalt-Doped Hematite Thin Films for Electrocatalytic Water Oxidation in Highly Acidic Media. *Chem. Commun.* **2019**, *55* (34), 5017–5020.

- (11) Yan, K.-L.; Chi, J.-Q.; Xie, J.-Y.; Dong, B.; Liu, Z.-Z.; Gao, W.-K.; Lin, J.-H.; Chai, Y.-M.; Liu, C.-G. Mesoporous Ag-Doped Co₃O₄ Nanowire Arrays Supported on FTO as Efficient Electrocatalysts for Oxygen Evolution Reaction in Acidic Media. *Renewable Energy* **2018**, *119*, 54–61.
- (12) Bloor, L. G.; Molina, P. I.; Symes, M. D.; Cronin, L. Low pH Electrolytic Water Splitting Using Earth-Abundant Metastable Catalysts That Self-Assemble in Situ. *J. Am. Chem. Soc.* **2014**, *136* (8), 3304–3311.
- (13) Zhu, Y.; Wang, J.; Koketsu, T.; Kroschel, M.; Chen, J.-M.; Hsu, S.-Y.; Henkelman, G.; Hu, Z.; Strasser, P.; Ma, J. Iridium Single Atoms Incorporated in Co₃O₄ Efficiently Catalyze the Oxygen Evolution in Acidic Conditions. *Nat. Commun.* **2022**, *13* (1), 7754.
- (14) Chong, L.; Gao, G.; Wen, J.; Li, H.; Xu, H.; Green, Z.; Sugar, J. D.; Kropf, A. J.; Xu, W.; Lin, X.-M.; Xu, H.; Wang, L.-W.; Liu, D.-J. La- and Mn-Doped Cobalt Spinel Oxygen Evolution Catalyst for Proton Exchange Membrane Electrolysis. *Science* **2023**, *380* (6645), 609–616.
- (15) Li, A.; Kong, S.; Guo, C.; Ooka, H.; Adachi, K.; Hashizume, D.; Jiang, Q.; Han, H.; Xiao, J.; Nakamura, R. Enhancing the Stability of Cobalt Spinel Oxide towards Sustainable Oxygen Evolution in Acid. *Nat. Catal.* **2022**, *5* (2), 109–118.
- (16) Wang, N.; Ou, P.; Miao, R. K.; Chang, Y.; Wang, Z.; Hung, S.-F.; Abed, J.; Ozden, A.; Chen, H.-Y.; Wu, H.-L.; Huang, J. E.; Zhou, D.; Ni, W.; Fan, L.; Yan, Y.; Peng, T.; Sinton, D.; Liu, Y.; Liang, H.; Sargent, E. H. Doping Shortens the Metal/Metal Distance and Promotes OH Coverage in Non-Noble Acidic Oxygen Evolution Reaction Catalysts. *J. Am. Chem. Soc.* **2023**, *145* (14), 7829–7836.